

Performance analysis of the European X-ray Free Electron Laser 3.9 GHz superconducting cavities

M. Bertucci, A. Bignami, A. Bosotti, P. Michelato, L. Monaco, C. Pagani,*
R. Paparella, and D. Sertore

INFN Sezione di Milano–Laboratorio LASA, Via Fratelli Cervi 201, 20090 Segrate (Mi), Italy

C. Maiano and P. Pierini

European Spallation Source ERIC, 22484 Lund, Sweden

J. Chen

Shanghai Institute of Applied Physics, Chinese Academy of Sciences, Shanghai 201800, China



(Received 3 January 2019; published 12 August 2019)

The limits of performance of the European XFEL 3.9 GHz superconducting cavities were investigated. Most cavities exhibited high field Q slope, reaching the breakdown field at approximately 22 MV/m. We hypothesize that this limit is a feature of high frequency cavities and can be explained by a thermal model incorporating field dependent surface resistance. The results obtained from simulations were in good agreement with experimental data obtained at 2 K.

DOI: [10.1103/PhysRevAccelBeams.22.082002](https://doi.org/10.1103/PhysRevAccelBeams.22.082002)

I. INTRODUCTION

Twenty third-harmonic 3.9 GHz superconducting cavities were fabricated and tested at LASA as part of the contribution of INFN and DESY to the European XFEL project (EXFEL). The third harmonic section of the XFEL injector serves to compensate the nonlinear distortion of longitudinal phase-space produced by the first acceleration stage. As a result the downstream bunch compression stage can deliver a higher current beam to the undulator section with improved transverse emittance. Two third-harmonic modules, each made of eight 3.9 GHz cavities, have already been assembled and one is currently in operation in the injector section of the machine.

In previous work, the cavity design, the fabrication and the qualification testing at LASA have been discussed [1]. In addition, there was a preliminary analysis of vertical test results and a first qualitative interpretation of the mechanism limiting the cavity performance at high fields [2]. Now, a more in-depth analysis is presented. The theoretical modeling of Q_0 vs E_{acc} is treated in detail and the quantitative predictions of this model are compared with the experimental results and data collected from cavity diagnostics.

*Also at Università degli Studi di Milano, Via Celoria 13, 20129 Milano, Italy.

Published by the American Physical Society under the terms of the Creative Commons Attribution 4.0 International license. Further distribution of this work must maintain attribution to the author(s) and the published article's title, journal citation, and DOI.

II. FABRICATION AND TESTING OF THE 3.9 GHz SERIES PRODUCTION CAVITIES

A. Production

Experience from 3.9 GHz series production has been described in detail in a previous paper [1]. We report here briefly only the main aspects involving the preparation of the rf surface. Due to their high frequency, 3.9 GHz cavities have a strong sensitivity to geometric variations arising from the fabrication and surface preparation process. Optimization and stabilization of the procedures have been achieved thanks to the previous experience of FNAL and DESY [3] during the development of the FLASH third-harmonic system (ACC39). The production of three preseries cavities allowed the optimization of the process using the infrastructure provided by the qualified industrial vendor. The niobium material used in these cavities was supplied by Ningxia OTIC in two different batches of 60 niobium sheets. Both batches met the required material specifications of $RRR > 300$, predominant grain size of $ASTM = 6$ or finer and no grains larger than $ASTM = 6$. Every sheet ($2.8 \text{ mm} \times 265 \text{ mm} \times 265 \text{ mm}$) was quality-checked at DESY by the Eddy Current Scanning technique.

After equatorial welding of dumbbells, the cavity inner surface underwent the following treatment steps: (i) Bulk buffered chemical polishing (BCP) at a 1:1:2 volume ratio. Approx. $124 \mu\text{m}$ of average thickness was removed in the first batch of 10 cavities. This was increased to $135 \mu\text{m}$ for the second batch. A typical etching rate of $1 \mu\text{m}/\text{min}$ to $1.4 \mu\text{m}/\text{min}$ was achieved in all treatments. The acid mixture was chilled to ensure that cavity

temperature was below 15 °C during the treatment. (ii) External surface BCP at a 1:1:2 volume ratio. Approx. 20 μm of surface was removed. (iii) Annealing for 2 hours in an oven at 800 °C to achieve hydrogen degassing. (iv) Final “Flash” BCP at a 1:1:2 volume ratio. Approximately 35 μm of surface was removed for the first batch of 10 cavities. This was reduced to 20 μm for the second batch. (v) High pressure rinse cycle. 12 hours at 100 bar with ultra pure water (UPW).

The bulk BCP process was performed in three steps to improve the uniformity of surface removal, reversing the cavity after each treatment. After each step, rinsing with UPW, weighing, drying, and frequency testing was performed in order to monitor the frequency response to the etching process. Two optical inspection processes—one immediately after electron beam welding and one after the 800 °C annealing—were performed to check for the presence of welding imperfections and large geometrical defects which could limit the cavity performance. These inspections revealed some suspect features close to welding seams in 7 cases, 6 after the EBW stage and one after the 800 °C annealing. In the latter case (cavity 3HZ004) the cavity underwent a further 15 min BCP treatment after grinding to remove the defect.

B. Vertical acceptance testing as performed at the LASA facility

The 20 series cavities were tested at the LASA vertical test facility to confirm the required EXFEL qualification values of $E_{\text{acc}} = 15 \text{ MV/m}$ and $Q_0 = 10^9$ at the operating temperature of 2 K. The test cryostat allowed testing of two cavities at a time. The accelerating field was raised until a limiting mechanism prevented any further power rise. Second sound and fast thermometry sensors were employed for the detection of quench events. An external proportional counter was installed above the cryostat for measuring x-ray radiation due to field emission. A mu-metal magnetic shield was installed, and a maximum value of 10 mG was measured in the cavity region with a fluxgate triaxial magnetometer. A full description of the test facility, together with cavity preparation for the tests have been reported [1]. After the 2 K characterization, the helium bath temperature was lowered to 1.8 K or below and the power rise repeated.

The cavity surface resistance $R_s(T) = R_{\text{BCS}}(T) + R_0$ was measured during the cool-down. SUPERFIT code [4] with the Halbritter quasiexponential formula for BCS surface resistance [5] was employed to separate the $R_{\text{BCS}}(T)$ (BCS resistance) and R_0 (residual resistance) contributions. Reduced band gap $\frac{\Delta}{k_B T_c}$, electron mean free path l_e and residual resistance R_0 were treated as free parameters in this fit, while $T_c = 9.25 \text{ K}$, $\lambda_l = 32 \text{ nm}$, and $\xi_0 = 39 \text{ nm}$ were used as fixed parameters for critical temperature, London penetration depth and coherence length, respectively.

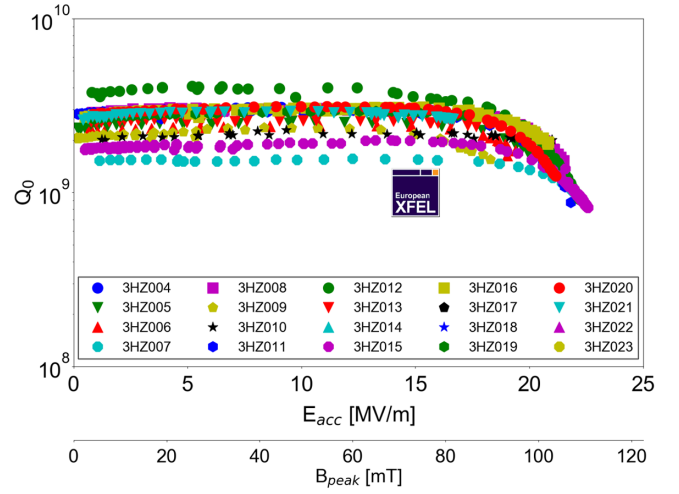


FIG. 1. Power rises for the 20 series production EXFEL 3.9 GHz cavities at 2 K. The qualification values ($E_{\text{acc}} = 15 \text{ MV/m}$ and $Q_0 = 10^9$) are also shown.

The fit results have been reported previously [2]. In summary, a large spread was obtained for residual resistance, with values ranging between 14 and 85 n Ω . With respect to BCS, the reduced band gap ranged between 1.78 and 1.90 and the electron mean free path ranged from 340 \AA (nearly the dirty limit) up to 2900 \AA (toward the clean limit). Assuming a first approximation $l_e = 27 \cdot \text{RRR}$ [6], this corresponded to a surface RRR in the 12-112 interval. Such a range of values, which is lower than the RRR bulk value of 300, may be justified by assuming a higher concentration of interstitials in the rf active layer. Experimental evidence of a near-surface hydrogen enriched layer with a thickness of about 100 \AA to 200 \AA has been reported following testing by the elastic recoil detection technique on niobium samples with treatment conditions similar to ours [7].

The power rises at 2 K for all the 20 cavities are shown in Fig. 1. A summary of cavity performance is outlined in Table I. Maximum accelerating field, Q_0 values at low (1 MV/m) and maximum accelerating field, and maximum external radiation (measured at the top of the cryostat) are shown.

All cavities except one met the EXFEL specifications, with the majority reaching 20 MV/m, or more. There was a large spread in the low field Q values, due to the related spread in residual resistance R_0 . With cavity 3HZ022, the observed anomalous value of $Q_0 = 4 \times 10^9$ is still under investigation. Regarding the performance at high fields, two different behaviors were observed: (i) Group I: Cavities 3HZ007, 3HZ010, 3HZ014, 3HZ019, 3HZ021, and 3HZ023 quenched all below 20 MV/m, with an average maximum E_{acc} of $16.6 \pm 1.5 \text{ MV/m}$. The high field Q-value was almost equal to the one at low field. There was a clear change of maximum E_{acc} with He bath temperature. Pointlike defects were detected by diagnostics. (ii) Group II: Cavities 3HZ004,

TABLE I. Performances of 3.9 GHz cavities.

Cavity name	$E_{\text{acc}}^{\text{max}}$ [MV/m]	Q_0 ($\times 10^9$) at 1 MV/m	Q_0 ($\times 10^9$) at $E_{\text{acc}}^{\text{max}}$	ext. rad. [$\mu\text{Sv/h}$]
3HZ004	20.0	2.03	0.99	No
3HZ005	20.1	2.39	1.65	No
3HZ006	20.9	2.30	2.02	No
3HZ007	19.7	2.59	2.31	No
3HZ008	21.0	2.39	1.51	No
3HZ009	18.3	2.12	1.56	No
3HZ010	18.2	1.56	1.55	No
3HZ011	21.8	2.68	0.88	2
3HZ012	20.8	2.69	2.12	No
3HZ013	22.0	1.93	0.98	No
3HZ014	15.0	2.91	2.89	No
3HZ015	22.3	2.06	1.03	No
3HZ016	21.1	2.74	1.90	No
3HZ017	22.1	1.56	0.95	No
3HZ018	21.8	2.63	1.46	No
3HZ019	17.0	2.70	2.67	No
3HZ020	21.0	2.72	1.26	0.2
3HZ021	18.0	2.70	2.63	No
3HZ022	22.1	4.11	0.93	No
3HZ023	17.8	2.54	2.39	No

3HZ005, 3HZ008, 3HZ011, 3HZ012, 3HZ013, 3HZ015, 3HZ016, 3HZ017, 3HZ018, 3HZ020, and 3HZ022 quenched above 20 MV/m, with an average maximum E_{acc} of 21.3 ± 0.8 MV/m. All exhibit a high field Q slope, which begins at about 17 MV/m. In some cases, this dramatically reduced the Q value to less than half of low field Q_0 . There was almost no change in maximum E_{acc} with He bath temperature. Cavity diagnostics did not identify any local quenches.

Outside the group I and group II behaviors were the cases of 3HZ006 and 3HZ009. Only a modest reduction of Q occurred at the quench field of 20.9 MV/m in the former. A significant Q drop occurred, even at the lower quench field of 18.3 MV/m, in the latter.

The difference of behavior is particularly evident when comparing the power rises at different temperatures. Figure 2 shows the power rises for cavity 3HZ021. An improvement of quench field for lower temperatures is evident, together with the increase in Q_0 value, as expected from BCS temperature dependence. A resistive defect, generating local thermal quench, is likely to be involved in the mechanism limiting cavity performance.

The power rises for cavity 3HZ015 at different bath temperatures are shown in Fig. 3. It is different from the previous case, with almost no gain in breakdown field at lower bath temperatures. The quench field at 1.7 K was only marginally higher than that at 2 K. Even more surprising, the Q value at maximum field was essentially the same at all temperatures. Every Q vs E_{acc} curve appears to converge in the same point, in spite of the difference in BCS resistance. In the insert, the power rise at 2 K is

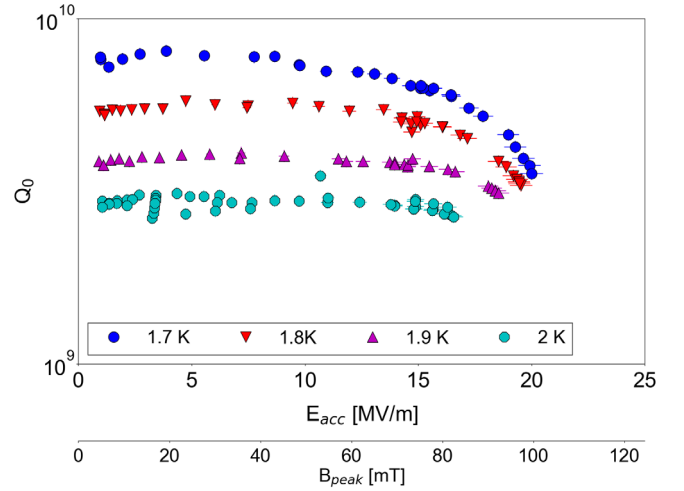
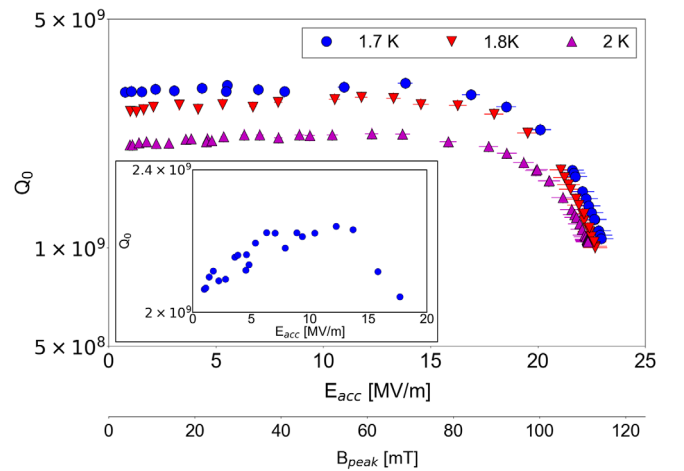


FIG. 2. Power rises for cavity 3HZ021 at different He bath temperatures.

magnified in the medium field zone. As also noticed by experiments at FNAL [8], BCP treated 3.9 GHz cavities exhibited a natural anti-Q slope at medium fields. In this case, we noticed a 10% increase of the initial value around 15 MV/m, in line with the previously mentioned experimental results. On the whole, the high field behavior of cavity 3HZ015—and all others from the 2nd group—appeared to be linked to thermal breakdown. The simple model of a resistive defect based mechanism does not provide a good explanation, as there is essentially no gain in breakdown field when decreasing the bath temperature. Moreover, the reduction of Q-value suggest a global mechanism of dissipation which is triggered well before the breakdown field. Ultimately, the narrow range of breakdown fields—a few tenths of MV/m around the average value of 21.3 MV/m—led us to suspect an innate limiting mechanism in the 3.9 GHz cavities prevailing at

FIG. 3. Power rises for cavity 3HZ015. In the box, the Q vs E_{acc} curve at 2 K is magnified in the 0–20 MV/m zone so to point out a slight medium field anti-Q slope.

that field. The lower breakdown field observed with group I cavities could be due to true pointlike defects that, if removed, would result in cavity performances similar to those of group II. The next section, which deals with diagnostics of quench events, will supply new evidence for these views.

C. Diagnostics for quench events

The process of thermal breakdown on the cavity inner surface leads to a great dissipation of heat at the Nb-He interface, synchronous with the drop of cavity transmitted power. This eventually increases the temperature of the surface and generates second sound shock waves in the superfluid helium. Both phenomena, if localized to a restricted area on the cavity surface, can be easily detected by means of fast thermometry and second sound sensors.

A thermometry sensor offers a means of directly identifying hot spot positions on the cavity surface but has a restricted spatial resolution. It is ineffective in detecting a quench if placed only few cm far away from the heat source. Therefore, an accurate thermometry mapping system needs to be employed incorporating several hundreds of sensors [9] in order to cover effectively the whole cavity active surface. Alternatively, a traditional second sound sensor—oscillating superleak transducer (OST) [10]—is able to detect the second sound waves coming from a wide area of the cavity surface, namely its whole line-of-sight. The simultaneous detection of the second sound signal by three sensors is therefore theoretically adequate to localize the quench position by means of trilateration.

In the case of 3.9 GHz cavities, due to their small size, it is advantageous to apply the second sound diagnostic technique. Such a sensor is able to cover, by line of sight, a large portion of the cavity surface if placed appropriately. On the other hand, several error sources can affect the quench localization accuracy, such as the extended active sensor surface, the sometimes difficult identification of second sound pulse wave front and even additional phenomena altering thermodynamic properties of superfluid helium, producing local variations of second sound velocity [11]. As a consequence, spatial resolution of the quench zone is limited to 5 mm-10 mm.

Given these considerations, we based our strategy for quench localization mainly on the second sound technique and less on fast thermometry, due to the limited number of available thermometry sensors. The visual inspection performed before testing gave an immediate indication of suspected points which could generate a thermal breakdown event. This provided the preferential sites for the placing of thermometry sensors. The second sound sensors were instead uniformly placed on the frame around the cavity, without any reference from optical inspection results. Thermometers (Cernox ® and CCS ®) with fast readout electronics were attached to the cavity surface, with a four-wire configuration to read the resistance of the

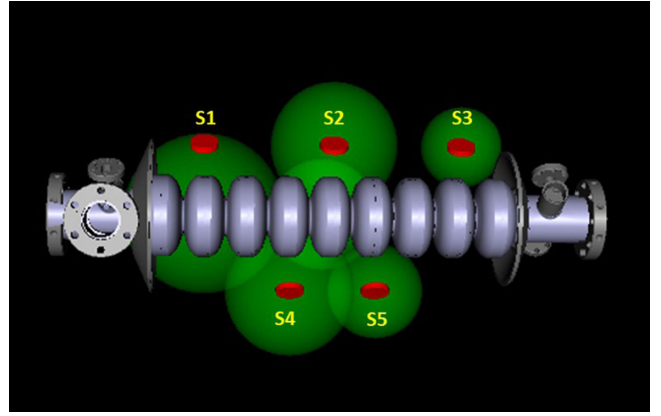


FIG. 4. Reconstruction of second sound signals for cavity 3HZ017. The spheres represent the quench detection range of the sensors.

sensor. In order to increase the reconstruction accuracy, 10 OST's were used for each cavity. Several algorithms of trilateration [12] were exploited for the reconstruction of the quench position.

Second sound signal analysis for cavities of group II (those quenching at high field with Q-slope) did not identify any isolated hot spots. Figure 4 shows a representative attempt to reconstruct a quench location for cavity 3HZ017 at 1.8 K. The spheres represent all points with a distance $d_i = v(1.8 \text{ K}) \cdot \Delta t_i$ from the sensor center, where $v(1.8 \text{ K})$ is the second sound velocity in superfluid helium at 1.8 K, and Δt_i is the measured time of arrival of second sound wave-front at the i th OST. For instance, sensor S3 points at cell 8 surface while S5 at cell 6, so it is unlikely that a single restricted zone on cavity surface would generate second sound waves.

Such behavior could be explained by assuming a global cavity heating mechanism as the trigger for second sound generation from high magnetic field zones near the cell equators. Conversely, group I cavities second sound signals are likely to come from a unique and well defined zone on the cavity surface.

Cavities 3HZ021 and 3HZ014 provided some interesting results. Cavity 3HZ021 prematurely quenched at 18 MV/m, well below the average accelerating field exhibited by the series production, without any associated significant Q value reduction. Figure 5 shows the results of the second sound quench reconstruction and the optical image of the quench area acquired after cavity welding. A shiny row, appearing just underneath the heat affected zone, is likely to be the source of cavity thermal breakdown. The defect was also present in the optical image taken after BCP treatment, confirming its role in the quench event.

Cavity 3HZ014 is the only one of the series production which did not meet, albeit marginally, the EXFEL specifications, with a quench event occurring at 15 MV/m without any reduction of Q-value. The result of second sound reconstruction is shown in Fig. 6 for a 1.8 K bath

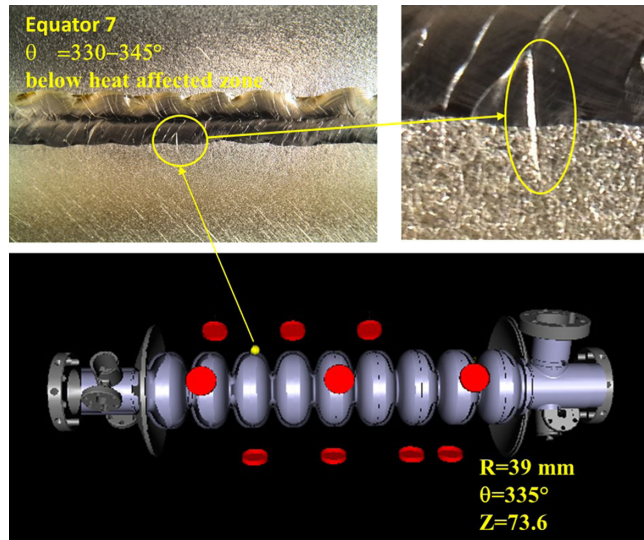


FIG. 5. Second sound quench reconstruction for cavity 3HZ021 (below) and optical image of the quench position (top left). On the top right, a magnification of the defect.

temperature, together with the corresponding optical image acquired in the inner cavity surface after 800°C heat treatment. Optical inspection of this cavity after BCP treatment revealed several bumps on the equatorial weld zone. They were not visible in the image acquired after welding, indicating that this is a feature of the BCP treatment itself. Being aware that these defects could produce a premature cavity quench, the fast thermometry sensor C1 (Echo) was placed at the defect position to allow monitoring of the local temperature response during the cavity power rise. Figure 7 shows the time response of fast thermometry sensors together with the rf gate (pulsed mode with 25% duty cycle) and transmitted power.

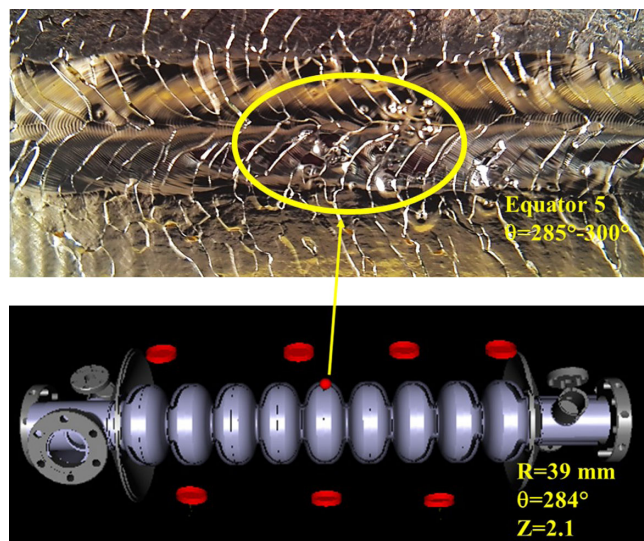


FIG. 6. Second sound quench reconstruction for cavity 3HZ014 (below) at 1.8 K and optical image of the quench position (top).

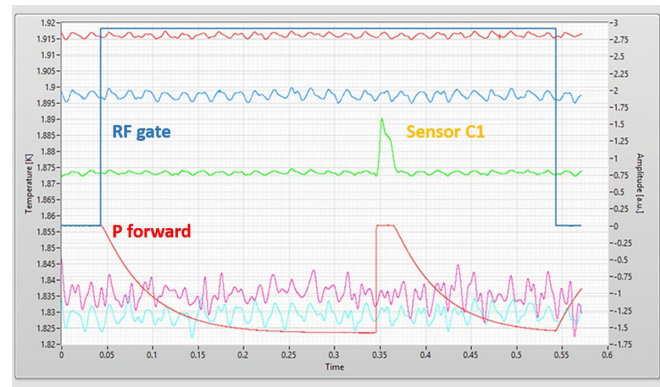


FIG. 7. Fast temperature sensors readout at the quench field. rf gate (violet) and transmitted power (red) and the sensor at the defect position (green) are highlighted.

Simultaneously with the drop of transmitted power (quench event), sensor C1 (Echo) registered a sudden temperature increase indicating a strong thermal transition on the cavity external surface, and an isolated hot spot generating second sound waves. This was associated with the premature thermal breakdown.

III. MECHANISM OF PERFORMANCE LIMITATION

A. General considerations

The quench behavior of the group I cavities at high field was different from that of group II. In the latter, a thermal breakdown was likely involved but there was no precise indication of a local hot spot. Several important clues were found from the analysis of power rises. There was an almost constant quench field in the interval 20–22 MV/m with an absence of any maximum gradient improvement with decreasing He bath temperature and a dramatic reduction of Q value while approaching the quench field. Putting this all together, a mechanism based on global thermal limitation can be suggested as the cause of gradient limitation for BCP treated 3.9 GHz cavities. This is also supported by similar results obtained by FNAL [13] in the development of FLASH third harmonic system. Even in that case, the occurrence of cavity quench at similar fields led to the conclusion of a possible global thermal dissipation. High field Q slope can be encountered in numerous situations, for different cavity frequencies and surface treatments [14–18]. To account for these observations, the mechanism of global thermal limitation in 3.9 GHz cavities, as distinct to lower frequency cavities, appears to be due to the fact that quenches due to local defects occur *above* the accelerating field that triggers the global thermal instability.

As a first attempt for analytically reconstructing the Q vs E_{acc} behavior, a simple thermal feedback model was used [19]. The temperature profile inside the cavity can be calculated by finding the equilibrium solution from the heat equation:

$$\rho C_v \frac{\partial T(\vec{r}, t)}{\partial t} = \nabla \cdot [k \nabla T(\vec{r}, t)] \quad (1)$$

where ρ is niobium density, C_v is niobium specific heat, k is the thermal conductivity. The following boundary conditions were applied to the Nb-vacuum and He-Nb interfaces, respectively:

$$-k \left. \frac{\partial T(z, t)}{\partial z} \right|_{z=0} = \frac{1}{2} R_s H_p^2 \quad (2)$$

$$-k \left. \frac{\partial T(z, t)}{\partial z} \right|_{z=d} = h_k [T(d, t) - T_0] \quad (3)$$

where R_s is the surface resistance, function of local temperature $T(0, t)$, H_p is peak surface magnetic field, T_0 is the He bath temperature, d is the wall thickness and h_k is Kapitza heat transfer coefficient, which is also a function of the local surface temperature $T(d, t)$. At equilibrium $\frac{\partial T(\vec{r}, t)}{\partial t} = 0$, so that Eq. (1) reduces to $\nabla \cdot [k \nabla T(\vec{r}, t)] = 0$, which can be solved by simple integration. Assuming small variations in temperature with respect to T_0 , thermal conductivity and the Kapitza heat transfer coefficient can be approximated by their value at T_0 . The cavity heat balance can be expressed by:

$$\frac{1}{2} R_s(T) H^2 = h(T_0)(T - T_0) \quad (4)$$

where $\frac{1}{h} = \frac{1}{h_k} + \frac{d}{k}$ is a thermal transport parameter—which is temperature dependent—and incorporates the combined effect of heat transfer in the lattice and interface heat transfer through the Kapitza mechanism. Equation (4) allows the evaluation of rf layer temperature T as a function of surface magnetic field H .

Starting from this model we performed an analytical reconstruction of the Q slope. Surface resistance was expressed as $R_s(T_0) = R_0 + R_{\text{BCS}}(T_0)$, where $R_{\text{BCS}}(T)$ was calculated using the classical quasi-exponential formula with a field-independent band-gap. Temperature dependent thermal conductivity was calculated with the analytic expression presented by Koechlin and Bonin [20], using RRR = 300 and phonon mean free path $l = 0.1$ mm. Several classical references for Kapitza heat transfer coefficient were employed. Here we report only the closest match so far obtained, with the Kapitza parameters coming from measurements on RRR 178 etched niobium samples [21]. Figure 8 shows the result for 3HZ015 at 2 K and 1.8 K.

It is evident that the thermal feedback model alone is not sufficient to fully reconstruct the Q slope of 3.9 GHz cavities. The large increase of surface resistance, more than doubling this value at 20 MV/m, is not achievable by ordinary heating of the rf surface. Moreover, according to this model the Q values start to decrease at low fields,

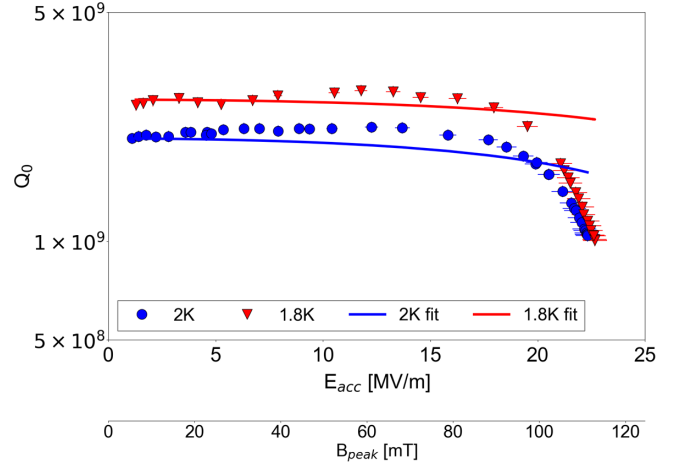


FIG. 8. Experimental and reconstructed Q vs E_{acc} curves for 3HZ015 at 2 K and 1.8 K.

whereas experimental Q-values were stable until a field of approximately 17 MV/m was reached.

B. The field-dependent BCS resistance model

We now consider the theory of dissipative nonlinear conductivity under strong magnetic fields, developed by Gurevich [22]. This introduces a nonlinear magnetic field dependence on surface resistance. The classical Mattis-Bardeen theory [23], which describes the response of a low temperature $T < T_c$ superconductor to an electromagnetic field, is generalized to the case of high fields, by taking into account the non-equilibrium behavior of quasiparticles. After being thermally excited, quasiparticles interact with the rf field of frequency ω through the absorption of energy quanta $E = \hbar\omega$. The quasiparticles are driven out of thermodynamic equilibrium by the presence of the screening currents, which broaden the density of states of the quasiparticles and reduce the band gap. A field-dependent quasiparticle gap $\epsilon_g(B) < \Delta_0$ is therefore defined as the maximum energy at which $N(\epsilon_g) = 0$. The strong rf field $B(t) = B_0 \cos(\omega t)$ produces a periodic smearing of quasiparticle energy gap from $\epsilon = \Delta$ when $B = 0$ to $\epsilon = \epsilon_g$ when $B = B_0$. As a consequence, surface conductivity is time-dependent. A new expression for nonlinear surface conductivity can be obtained by time averaging the rf cycle:

$$\sigma_1(B) = \frac{2\sigma_n}{\pi\hbar} \int_0^{\frac{\pi}{\omega}} dt \int_{\epsilon_g(t)}^{\infty} [f(\epsilon, s) - f(\epsilon + \hbar\omega, s)] M d\epsilon \quad (5)$$

where σ_n is normal state surface conductivity, $f(\epsilon, s)$ is the energy distribution of quasiparticles, $s = s(x, t) = \Delta_0 \left[\frac{B(t)e^{-x/\lambda}}{2B_c} \right]^2$ is the screening current at a depth x from the rf surface, λ the London penetration depth, B_c the thermodynamic critical field, and $M(\epsilon, \omega, B)$ is a spectral function. Surface resistance is then evaluated as:

$$R_s(B) = \frac{\mu_0^2 \omega^2 \lambda^3}{2\beta_0} \int_0^{\beta_0} \sigma_1(\beta) d\beta \quad (6)$$

where $\beta_0 = [\frac{B_0}{2B_c}]^2$.

In this mode, the current induced broadening of quasiparticle density of states produces a significant decrease in surface conductivity. This is the favorable side of the nonequilibrium, reducing the value of surface resistance with respect to the predictions of the Mattis-Bardeen theory. Such a mechanism has been employed to explain the anti-Q slope behavior of nitrogen-doped cavities [24,25]. On the other hand, the function $f(\epsilon, s)$ in Eq. (5) is different from Fermi-Dirac distribution, which assumes the thermodynamical equilibrium: conversely, it is a complex nonequilibrium distribution accounting for the kinetic balance of the rf power absorption, the recombination of quasiparticles into Cooper pairs and the inelastic scattering of quasiparticles with phonons of niobium lattice. However, typical times for inelastic quasiparticle-phonon scattering and Cooper pair recombination at 2K for niobium are $\tau_s = 1.7 \times 10^{-8}$ s and $\tau_r \approx 0.4 \times 10^{-6}$ s, respectively, which are two orders of magnitude greater than the characteristic rf period; that for 3.9 GHz frequency is 2.56×10^{-10} s. This means that quasiparticles do not have enough time to exchange energy with the lattice and change their density during the rf cycle. Hence the quasiparticle temperature, which is higher than the lattice temperature, remains stable during the rf cycle and a static energy distribution can be analytically deduced as function of quasiparticle temperature $f(\epsilon, T)$. This effect, known as quasiparticle overheating, represents the adverse effect of the nonequilibrium behavior. This leads to quasiparticles temperature higher than lattice temperature. Thus, a new term accounting for heat transfer between overheating quasiparticles and lattice phonons has to be considered in the whole cavity heat balance. Thus:

$$\frac{1}{2} R_s(H, T) H^2 = Y(T - T_i) \quad (7)$$

$$Y(T - T_i) = h(T_i - T_0) \quad (8)$$

where $R_s(H, T) = R_0 + R_{BCS}(H, T)$, with field dependent BCS resistance expressed by Eq. (6), T is quasiparticle temperature, T_i the lattice temperature, h is the thermal coefficient already defined in Eq. (4), and Y is a term quantifying the quasiparticle-phonon transfer rate. Eventually, assuming that $T - T_0 \ll T_0$ the set in Eq. (7) reduces to:

$$\frac{1}{2} R_s(H, T) H^2 = \frac{1}{\alpha'} (T - T_0) \quad (9)$$

where the parameter $\alpha' = \frac{1}{Y} + \frac{1}{h} = \frac{1}{Y} + \frac{1}{h_K} + \frac{d}{k}$ known as the normalized overheating parameter, encloses all material parameters: the quasiparticle-phonon energy transfer

through Y , the heat conduction in the bulk through the thermal conductivity k , and the heat transfer in the Nb-He interface through the Kapitza mechanism h_K . Together with Eqs. (6), (9) allows the calculation of the quasiparticle temperature and the determination of a self-consistent field-dependent surface resistance.

A more in-depth theoretical treatment of the field-dependent BCS resistance is found in [22], where the analytical expressions of all the above mentioned parameters, such as quasiparticle distribution, field-dependent energy gap and spectral function, are rigorously defined. The same model was used here to analyze the behavior of 3.9 GHz cavities at high field. Such an approach applies mainly to dirty superconductors which is not truly our case, but we assume the cavity rf surface is nearer to the dirty limit ($l_e < \xi_0$) than to clean limit ($l_e \gg \xi_0$) since, as reported in [2], $l_e \sim \xi_0$ for most of the cavities.

The role of the overheating parameter is crucial for the quantitative evaluation of surface resistance as a function of accelerating field. Unfortunately no simple analytical expression, nor experimental measurement, is available at high magnetic fields for the quasiparticle-phonon energy transfer coefficient Y , as its value is also influenced by the effect of local inhomogeneities and impurities. For this reason, α' is regarded in practical calculations as a free parameter. Thus, the Q vs E_{acc} experimental curve is compared with the reconstructed $Q(E_{acc}, \alpha')$ and the closest match is chosen as the true value for the overheating parameter.

If global thermal breakdown is assumed to be the limiting mechanism, the breakdown field, H_b , defined as the highest magnetic field for which Eq. (9) has a solution as a function of T , provides an additional constraint. Figure 9 shows the two terms of Eq. (9) as function of quasiparticle temperature, in the three cases $H < H_b$, $H = H_b$ and $H > H_b$.

For $H < H_b$, the solution is the intersection of the line $\frac{1}{\alpha'} (T - T_0)$ with the dissipated power term $\frac{1}{2} R_s(H, T) H^2$ expressed as function of temperature. For $H > H_b$, the dissipated power overwhelms the heat transport term and the system is thermally unstable. For $H = H_b$, the two curves are tangent for $T_{max} = T_{eq}(H_b)$. This means that not only the two terms in Eq. (9) are equal, but also their temperature derivatives:

$$\left. \frac{1}{2} \frac{dR_s(H_b, T)}{dT} \right|_{T_{max}} H_b^2 = \frac{1}{\alpha'} \quad (10)$$

Substituting α' in Eq. (9) and rearranging, one obtains:

$$R_s(H_b, T_{max}) = \left. \frac{dR_s(H_b, T)}{dT} \right|_{T_{max}} (T_{max} - T_0) \quad (11)$$

which allows calculation of T_{max} , and then from Eq. (9) the overheating parameter α' .

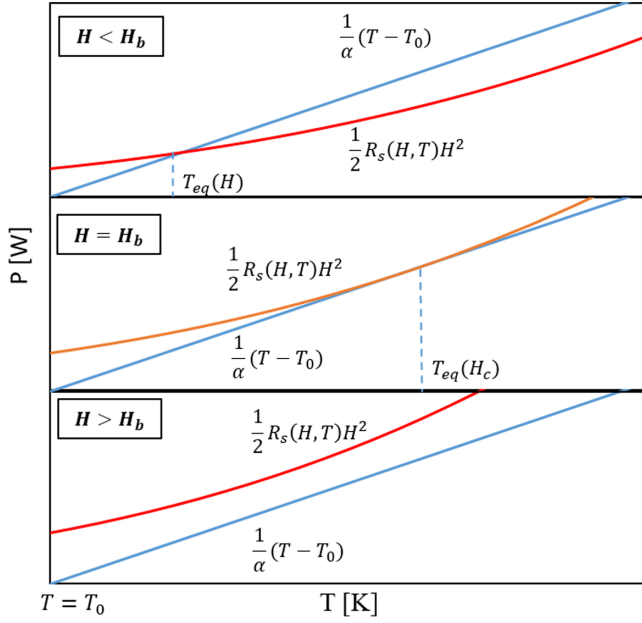


FIG. 9. Dissipated power and heat transport term versus quasiparticle temperature, in the three cases $H < H_b$, $H = H_b$, and $H > H_b$. Equilibrium temperature is at the intersection of the two curves.

In summary, if the experimentally measured quench field is considered as the global thermal breakdown gradient limit, one can deduce the overheating parameter from the solution of Eq. (11). It must be stressed, however, that a temperature independent overheating parameter needs to be assumed. The accuracy of this method needs to be checked in the case of high quasiparticle overheating.

C. Simulation results and discussion

The derivation of the XFEL 3.9 GHz cavities experimental Q vs E_{acc} curves with the field-dependent surface resistance model was performed as follows: (i) Experimental values for R_0 and R_{BCS} at low field were extracted from experimental data. The values used for each cavity were as reported previously [1]. The measured quench field was assumed to be the value triggering the global instability, namely the breakdown field H_b as defined in Eq. (10). (ii) Field dependent surface resistance given by Eq. (6) was calculated at $H = H_b$ and the function of temperature $R_s(H_b, T)$ was derived. T_{max} and α' were experimentally calculated from Eq. (11). (iii) Having calculated the overheating parameter, the surface resistance at different fields was calculated with Eq. (9). The Q value was calculated as $Q_0(E_{\text{acc}}) = \frac{G}{R_{\text{BCS}}(E_{\text{acc}}) + R_0}$, where G is the cavity geometry factor. As R_{BCS} is the dominant contribution to total surface resistance due to its f^2 dependence, we neglected any field dependence of the residual resistance term. Figure 10 shows the results of the reconstruction performed for cavity 3HZ015 at 2 K, 1.8 K, and 1.7 K, compared with the

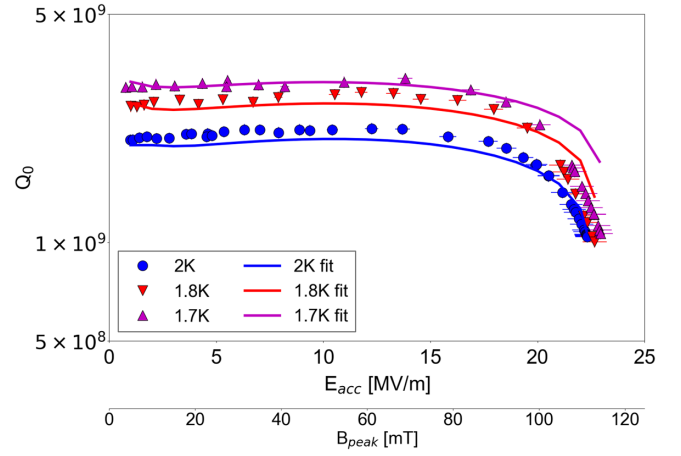


FIG. 10. Comparison between measured and calculated (fit) Q_0 vs E_{acc} curves for cavity 3HZ015 at 2 K, 1.8 K, and 1.7 K.

experimental Q vs E_{acc} curves. A 5% relative error was assumed for both the experimental values of Q_0 and E_{acc} [26]. The error of the calculated Q_0 was evaluated by means of error propagation assuming 5%, 5%, and 10% as the relative errors for E_{acc} , low field R_{BCS} and R_0 , respectively. For the sake of legibility, error bars are omitted from the graph.

There was a good agreement of the model results with experimental data at 2 K. The prediction of the model for both the Q slope and Q-value at breakdown field matched well with the corresponding experimental values. For 1.8 K and 1.7 K, the model underestimated the measured decrease of Q_0 with increasing accelerating field. The spread between experimental and simulated values is nevertheless noticeably decreased when compared to that of the thermal feedback model.

A slight increase of Q at medium field was also noticed. Calculated values ranged from 1.9×10^9 at 3 MV/m to 2.07×10^9 at 15 MV/m, similar to what happens in experimental data. The increase was 5% for the simulation, slightly less than the experimentally observed 8% increase. The mechanism accounting for this slight anti-Q slope could be the same that activates the vigorous anti-Q slope of nitrogen doped cavities.

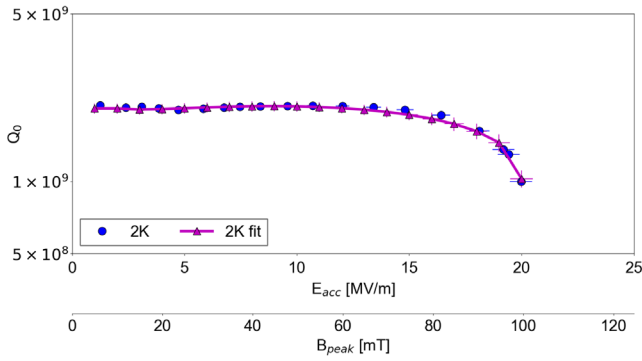
The values of α' for cavity 3HZ015 at the different temperatures are reported in Table II. A slight dependence of the overheating parameter on temperature can be noticed, consistent with the results obtained by others [24].

TABLE II. α' versus Helium bath temperature.

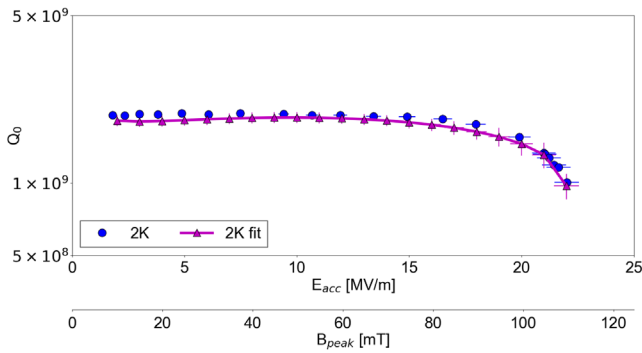
He bath temp. [K]	α' [$\text{m}^2\text{K}/\text{W}$]
1.7	0.52
1.8	0.48
2.0	0.44

Very similar values were obtained for the other 3.9 GHz series cavities, with some exceptions.

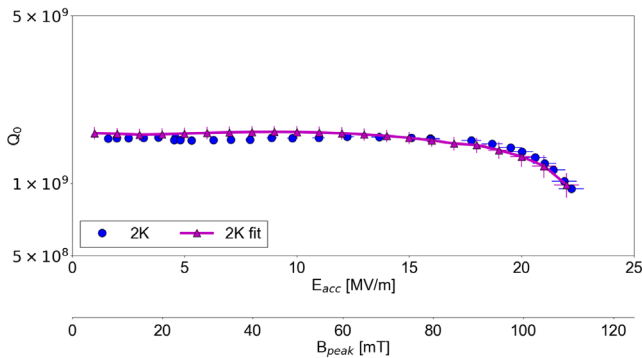
Figure 11 shows the results of the reconstruction for other 3.9 GHz series cavities at 2 K. 3HZ013 and 3HZ017 have critical fields close to that of 3HZ015, as shown by the calculated α' . However, cavity 3HZ004 quenched at 20 MV/m with a full Q-slope behavior. The estimated overheating parameter was higher, although treatment and materials used were the same as in other series cavities. Looking back to the processing experience reported in [1], cavity 3HZ004 was BCP treated at the beginning of the first batch, when



(a) 3HZ004. $\alpha = 0.53 \cdot 10^{-3} \frac{\text{m}^2\text{K}}{\text{W}}$, $E_{max} = 20 \frac{\text{MV}}{\text{m}}$



(b) 3HZ013. $\alpha = 0.44 \cdot 10^{-3} \frac{\text{m}^2\text{K}}{\text{W}}$, $E_{max} = 22.0 \frac{\text{MV}}{\text{m}}$



(c) 3HZ017. $\alpha = 0.40 \cdot 10^{-3} \frac{\text{m}^2\text{K}}{\text{W}}$, $E_{max} = 22.2 \frac{\text{MV}}{\text{m}}$

FIG. 11. Comparison between measured and calculated Q_0 vs E_{acc} curves for cavity 3HZ004 (a), 3HZ013 (b), and 3HZ017 (c) at 2 K. Errors on calculated value are also indicated. The estimated overheating parameters and the breakdown fields are reported in the subcaption.

treatment parameters were still not optimized. For example, the nominal acid flow had not yet been set at 1.5 L/min. This could explain the slight difference in performance of this cavity and may suggest an influence of final BCP treatment on the high field Q slope behavior.

It is worthwhile to evaluate the weight of each single heat transport contribution to the normalized overheating parameter. Employing the classical values of $k = 75 \text{ W}/(\text{mK})$ for thermal conductivity, $h_K = 1 \times 10^4 \text{ W}/(\text{m}^2\text{K})$ for Kapitza heat transfer coefficient, and $d = 2.6 \text{ mm}$ as wall thickness, one obtains $\frac{1}{h} = \frac{1}{h_K} + \frac{d}{k} \approx 0.13 \times 10^{-3} \text{ W}/(\text{m}^2\text{K})$. Hence, the quasiparticle-phonon energy transfer coefficient can be estimated as $\frac{1}{\gamma} = \alpha' - \frac{1}{h} \approx 0.31 \times 10^{-3} \text{ m}^2\text{K}/\text{W}$. It contributes 70% to the overheating normalized parameter. This means that the true bottleneck in cavity heat transfer is the quasiparticle-phonon interaction. In fact the temperature of the rf layer is higher due to the low efficiency of quasiparticles in reaching thermodynamic equilibrium with the lattice. The experimentally observed linear dependence of $\frac{1}{\gamma}$ to electron mean free path suggests a crucial role for impurities in moderating quasiparticle energy. An impurity embedded in the lattice may act as a scattering center for quasiparticles and favor energy transfer with lattice phonons.

The discrepancies observed between experimental and calculated values at lower temperatures deserves some comment. Several assumptions were made in order to apply the field-dependent surface resistance model to the experimental results. Specifically, this involved the linearization of the heat transport term allowing, through Eq. (11), to evaluate the overheating coefficient α as the derivative of $R(H_b, T)$ at the breakdown temperature. Such an approach cannot be used without this assumption. There is a need to know the temperature dependence of α' in order to generalize Eq. (11) to the case of temperature-dependent overheating. Within this constraint, linearization offers an initial means of assessing of the limiting performance of cavities at 2 K.

Several other approximations are intrinsic in the field-dependent surface resistance model. These include no simple analytical expression for field dependent band gap existing in the clean limit. The field dependence for band gap takes into account only the quadratic field correction. The nonlinear Meissner effect, introduces a field dependence for London penetration depth. The effect of surface roughness, which is known to be influential on performance limiting mechanisms, should also be carefully considered. The enhancement of surface magnetic field due to the rough BCP-treated surface can locally increase the dissipated power and therefore introduce an additional contribution to the Q-slope [27]. Finally, the residual resistance due to trapped magnetic flux is also field dependent [28,29], and is likely to influence the high-field Q behavior in interplay with BCS surface resistance. In the case of 3.9 GHz, assuming a trapping flux sensitivity of

0.5 n Ω /mG at low E_{acc} for a BCP-treated cavity [30], an external field of 10 mG would give an overall contribution of 5 n Ω to low-field surface resistance. Even assuming a worst case scenario where the trapped flux sensitivity reaches 1.5 n Ω /mG at 20 Mv/m, as pointed out in [30], the trapped flux contribution to residual resistance would not be more than 15 n Ω . Hence, the BCS surface resistance—which is of the order of 100 n Ω —would overwhelm any contribution of trapped magnetic flux, and at 2K one can neglect its dependence on magnetic field. Alternatively, at lower temperatures $R_{\text{BCS}}(T)$ decreases, eventually approaching a magnitude equivalent to the residual resistance. This may be a possible explanation of the discrepancies observed in our model at lower temperatures. In the future, the model will be extended to incorporate the most recent theories for the field dependence of sensitivity to trapped flux.

IV. CONCLUSIONS

The results of vertical cold tests of the 3.9 GHz superconducting cavities for the European XFEL were analyzed and a mechanism to explain the limits in cavity performance has been proposed.

A global thermal dissipation mechanism was identified, accounting for limiting of performance at approximately 22 Mv/m. Pivotal was the triggering of a high field Q slope starting from 17 Mv/m, induced by the high surface resistance (because of the f^2 dependence of $R_{\text{BCS}}(T)$). The high-field behavior was quantitatively reconstructed by only considering nonequilibrium superconductivity. High frequency plays a significant role in the overheating of the rf surface due to the kinetic balance between the short rf period of quasiparticle recombination and quasiparticle-phonon scattering. The fit results matched the experimental data at 2K. The discrepancies at lower temperatures could be due to the field dependence of residual resistance, which was not included. An upgrade of the mathematical model taking into account this contribution will be undertaken in the future.

Performance of the cavities clearly is dependent on surface treatment, which in this case was based on BCP. The BCP recipe employed is not optimal for achieving state-of-the-art performances but it was motivated by the need to meet the moderate specification value of 15 Mv/m for the XFEL third harmonic cavities. One would expect different breakdown fields and Q-slope onsets with different treatments. These could include a low temperature baking and using electropolishing bulk treatment with nitrogen doping. In the future, we plan to use these alternative treatments on 3.9 GHz cavities to investigate the influence of the surface preparation on the field-dependent surface resistance.

vertical test experience of the European X-ray Free Electron Laser 3.9 GHz superconducting cavities, *Phys. Rev. Accel. Beams* **20**, 042006 (2017).

- [2] M. Bertucci, A. Bignami, A. Bosotti, J. Chen, C. Maiano, P. Michelato, L. Monaco, R. Paparella, P. Pierini, D. Sertore, and C. Pagani, in *Proc. of the ninth Particle Accelerator Conference (IPAC'18), Vancouver, BC, Canada, April 29–May 4, 2018*, International Particle Accelerator Conference No. 9, JACoW (JACoW publishing, Geneva, Switzerland, 2018) p. 2644.
- [3] E. Vogel *et al.*, in *Proc. of International Particle Accelerator Conference (IPAC'10), Kyoto, Japan, May 23–28, 2010*, International Particle Accelerator Conference No. 1, JACoW (JACoW publishing, Geneva, Switzerland, 2010) pp. 4281–4283.
- [4] G. Ciovati, SUPERFIT: A computer code to fit surface resistance and penetration depth of a superconductor, JLAB Technical Report No. TN 03-003, 2003.
- [5] H. Padamsee, J. Knobloch, and T. Hays, *RF Superconductivity for Accelerators*, Wiley Series in Beam Physics and Accelerator Technology (Wiley, New York, 1998), p. 88.
- [6] B. Bonin, in *Proceedings of Cern Accelerator School—Superconductivity in Particle Accelerators Haus Rissen, Hamburg, Germany, 1995*, 96-03 (CERN, Geneva, 1996), p. 195.
- [7] A. Romanenko and L. V. Goncharova, in *Proc. of 15th International Conference on RF Superconductivity (SRF '11), Chicago, Illinois, USA, July 25–29, 2011*, International Conference on RF Superconductivity No. 15, JACoW (JACoW publishing, Geneva, Switzerland, 2012), p. 849.
- [8] M. Martinello, M. Checchin, A. Romanenko, A. Grassellino, S. Aderhold, S. K. Chandrasekaran, O. Melnychuk, S. Posen, and D. A. Sergatskov, Field-Enhanced Superconductivity in High-Frequency Niobium Accelerating Cavities, *Phys. Rev. Lett.* **121**, 224801 (2018).
- [9] M. Ge, G. Hoffstaetter, F. Furuta, E. Smith, M. Liepe, S. Posen, H. Padamsee, D. Hartill, and X. Mi, in *Proc. of North American Particle Accelerator Conference (NA-PAC '13), Pasadena, CA, USA, Sep. 29–Oct. 4, 2013*, North American Particle Accelerator Conference No. 2, JACoW (JACoW publishing, Geneva, Switzerland, 2014), p. 805.
- [10] R. A. Sherlock and D. O. Edwards, Oscillating superleak second sound transducers, *Rev. Sci. Instrum.* **41**, 1603 (1970).
- [11] P. Zhang and M. Murakami, Three dimensionality of pulsed second-sound waves in He II, *Phys. Rev. B* **74**, 024528 (2006).
- [12] M. Bertucci, A. Bosotti, L. Garolfi, P. Michelato, L. Monaco, D. Sertore, and C. Pagani, in *Proc. of 16th International Conference on RF Superconductivity (SRF '13), Paris, France, Sept. 23–27, 2013*, International Conference on RF Superconductivity No. 16, JACoW (JACoW publishing, Geneva, Switzerland, 2014) p. 710.
- [13] E. Harms, H. Edwards, A. Hocker, T. Khabiboulline, and N. Solyak, in *Proc. of the 24th Linear Accelerator Conference (LINAC '08), Victoria, British Columbia, Canada, Sept. 29–Oct. 3, 2008*, International Conference on Linear Accelerator No. 24, JACoW (JACoW publishing, Geneva, Switzerland, 2008), pp. 845–847.

[1] P. Pierini, M. Bertucci, A. Bosotti, J. Chen, C. G. Maiano, P. Michelato, L. Monaco, M. Moretti, P. Pagani, R. Paparella, D. Sertore, and E. Vogel, Fabrication and

- [14] J. Vines, Y. Xie, and H. Padamsee, in *Proc. of 13th International Conference on RF Superconductivity (SRF2007), Beijing, China, Oct. 14–19, 2007*, International Conference on RF Superconductivity No. 24, JACoW (JACoW publishing, Geneva, Switzerland, 2007), p. 178.
- [15] G. Ciovati and J. Halbritter, Analysis of the medium field Q-slope in superconducting cavities made of bulk niobium, *Physica C* **441**, 57 (2006).
- [16] L. Lilje, D. Reschke, K. Twarowsky, P. Schmüser, D. Bloess, E. Haebel, E. Chiaveri, J. M. Tessier, H. Preis, H. Wenninger, H. Safa, and J. P. Charrier, in *Proc. of International Conference on RF Superconductivity (SRF1999), Santa Fe, NM, USA, Nov. 1–5, 1999*, International Conference on RF Superconductivity No. 9, JACoW (JACoW publishing, Geneva, Switzerland, 1999), p. 74.
- [17] G. Ciovati, G. Ereemeev, and F. Hannon, High field Q slope and the effect of low-temperature baking at 3 GHz, *Phys. Rev. Accel. Beams* **21**, 012002 (2018).
- [18] P. Dhakal, G. Ciovati, and G. R. Myneni, Role of thermal resistance on the performance of superconducting radio frequency cavities, *Phys. Rev. Accel. Beams* **20**, 032003 (2017).
- [19] A. Gurevich, *Physica C* **441**, 38 (2006).
- [20] F. Koechlin and B. Bonin, Parametrization of the niobium thermal conductivity in the superconducting state, *Supercond. Sci. Technol.* **9**, 453 (1996).
- [21] H. Edwards, C. A. Cooper, M. Ge, I. V. Gonin, E. R. Harms, T. N. Khabiboulline, and N. Solyak, in *Proc. 14th International Conference on RF Superconductivity (SRF '09), Berlin, Germany, September 20–25, 2009*, International Conference on RF Superconductivity No. 14, JACoW (JACoW publishing, Geneva, Switzerland, 2009), p. 379.
- [22] A. Gurevich, Reduction of Dissipative Nonlinear Conductivity of Superconductors by Static and Microwave Magnetic Fields, *Phys. Rev. Lett.* **113**, 087001 (2014).
- [23] D. C. Mattis and J. Bardeen, Theory of the anomalous skin effect in normal and superconducting metals, *Phys. Rev.* **111**, 412 (1958).
- [24] J. T. Maniscalco, D. Gonnella, and M. Liepe, The importance of the electron mean free path for superconducting radio-frequency cavities, *J. Appl. Phys.* **121**, 043910 (2017).
- [25] M. Martinello, S. Aderhold, S. K. Chandrasekaran, M. Checchin, A. Grassellino, O. Melnychuk, S. Posen, A. Romanenko, and D. Sergatskov, in *Proceedings of the 18th International Conference on RF Superconductivity (SRF2017), Lanzhou, China, July 17–21, 2017*, International Conference on RF Superconductivity No. 18, JACoW (JACoW publishing, Geneva, Switzerland, 2018), p. 364.
- [26] O. Melnychuk, A. Grassellino, and A. Romanenko, Error analysis for intrinsic quality factor measurement in superconducting radio frequency resonators, *Rev. Sci. Instrum.* **85**, 124705 (2014).
- [27] C. Xu, C. E. Reece, and M. J. Kelley, Simulation of nonlinear superconducting rf losses derived from characteristic topography of etched and electropolished niobium surfaces, *Phys. Rev. Accel. Beams* **19**, 033501 (2016).
- [28] A. Romanenko and A. Grassellino, Dependence of the microwave surface resistance of superconducting niobium on the magnitude of the rf field, *Appl. Phys. Lett.* **102**, 252603 (2013).
- [29] C. Benvenuti, S. Calatroni, I. Campisi, P. Darriulat, M. A. Peck, R. Russo, and A.-M. Valente, Study of the surface resistance of superconducting niobium films at 1.5 GHz, *Physica C* **316**, 153 (1999).
- [30] M. Checchin, M. Martinello, A. Grassellino, S. Aderhold, K. Chandrasekaran, O. Melnychuk, S. Posen, A. Romanenko, and D. A. Sergatskov, Frequency dependence of trapped flux sensitivity in SRF cavities, *Appl. Phys. Lett.* **112**, 072601 (2018).